E89-003 PRC Article: V01 - work in progress

K. G. Fissum,[17] B. D. Anderson,[13] K. A. Aniol,[2] L. Auerbach,[29] F. T. Baker,[7] J. Berthot,[1] W. Bertozzi,[17] P. -Y. Bertin,[1] L. Bimbot,[22] W. U. Boeglin,[5] E. J. Brash,[24] V. Breton,[1] H. Breuer,[16] E. Burtin,[26] J. R. Calarco,[18] L. Cardman,[30] G. D. Cates,[23] C. Cavata,[26] C. C. Chang,[16] J. -P. Chen,[30] E. Cisbani,[12] D. S. Dale,[14] R. De Leo,[10] A. Deur,[1] B. Diederich,[21] P. Djawotho,[33] J. Domingo,[30] B. Doyle,[14] J. -E. Ducret,[26] M. B. Epstein,[2] L. A. Ewell,[16] J. M. Finn,[33] H. Fonvieille,[1] B. Frois,[26] S. Frullani,[12] J. Gao,[17] F. Garibaldi,[12] A. Gasparian,[8,14] S. Gilad,[17] R. Gilman,[25,30] A. Glamazdin,[15] C. Glashausser,[25] J. Gomez,[30] V. Gorbenko,[15] T. Gorringe,[14] F. W. Hersman,[18] R. Holmes,[28] M. Holtrop,[18] N. d'Hose,[26] C. Howell,[4] G. M. Huber,[24] C. E. Hyde-Wright,[21] M. Iodice,[12] C. W. de Jager,[30] S. Jaminion,[1] M. K. Jones,[33] K. Joo,[32] C. Jutier,[1,21] W. Kahl,[28] S. Kato,[34] J. J. Kelly,[16] S. Kerhoas,[26] M. Khandaker,[19] M. Khayat,[13] K. Kino,[31] W. Korsch,[14] L. Kramer,[5] K. S. Kumar,[23] G. Kumbartzki,[25] G. Laveissière,[1] A. Leone,[11] J. J. LeRose,[30] L. Levchuk,[15] M. Liang,[30] R. A. Lindgren,[32] N. Liyanage,[17] G. J. Lolos,[24] R. W. Lourie,[27] R. Madey,[8,13,30] K. Maeda,[31] S. Malov,[25] D. M. Manley,[13] D. J. Margaziotis[2] P. Markowitz,[5] J. Martino,[26] J. S. McCarthy,[32] K. McCormick,[21] J. McIntyre,[25] R. L. J. van der Meer,[24] Z. -E. Meziani,[29] R. Michaels,[30] J. Mougey,[3] S. Nanda,[30] D. Neyret,[26] E. A. J. M. Offermann,[30] Z. Papandreou,[24] C. F. Perdrisat,[33] R. Perrino,[11] G. G. Petratos,[13] S. Platchkov,[26] R. Pomatsalyuk,[15] D. L. Prout,[13] V. A. Punjabi,[19] T. Pussieux,[26] G. Quéméner,[33] R. D. Ransome,[25] O. Ravel,[1] Y. Roblin,[1] R. Roche,[6] D. Rowntree,[17] G.A. Rutledge,[33] P. M. Rutt,[30] A. Saha,[30] T. Saito,[31] A. J. Sarty,[6] A. Serdarevic-Offermann,[24] T. P. Smith,[18] A. Soldi,[20] P. Sorokin,[15] P. Souder,[28] R. Suleiman,[13] J. A. Templon,[7] T. Terasawa,[31] L. Todor,[21] H. Tsubota,[31] H. Ueno,[34] P. E. Ulmer,[21] G.M. Urciuoli,[12] P. Vernin,[26] S. van Verst,[17] B. Vlahovic,[20] H. Voskanyan,[35] J. W. Watson,[13] L. B. Weinstein,[21] K. Wijesooriya,[33] R. Wilson,[9] B. Wojtsekhowski,[30] D. G. Zainea,[24] V. Zeps,[14] J. Zhao,[17] Z. -L. Zhou[17]

(The Jefferson Lab Hall A Collaboration)

J. M. Udìas,[36] J. R. Vignote[36]

[1]Université Blaise Pascal/IN2P3, F-63177 Aubière, France

[2]California State University, Los Angeles, California, 90032, USA

[3]Institut des Sciences Nucléaires, F-38026 Grenoble, France

[4]Duke University, Durham, North Carolina, 27706, USA

[5]Florida International University, Miami, Florida, 33199, USA

[6]Florida State University, Tallahassee, Florida, 32306, USA

[7]University of Georgia, Athens, Georgia, 30602, USA

[8]Hampton University, Hampton, Virginia, 23668, USA

[9]Harvard University, Cambridge, Massachusetts, 02138, USA

[10]INFN, Sezione di Bari and University of Bari, I-70126 Bari, Italy

[11]INFN, Sezione di Lecce, I-73100 Lecce, Italy

[12]INFN, Sezione Sanitá and Istituto Superiore di Sanitá, Laboratorio di Fisica, I-00161 Rome, Italy

[13]Kent State University, Kent, Ohio, 44242, USA

[14]University of Kentucky, Lexington, Kentucky, 40506, USA

[15]Kharkov Institute of Physics and Technology, Kharkov 310108, Ukraine

[16]University of Maryland, College Park, Maryland, 20742, USA

[17]Massachusetts Institute of Technology, Cambridge, Massachusetts, 02139, USA

[18]University of New Hampshire, Durham, New Hampshire, 03824, USA

[19]Norfolk State University, Norfolk, Virginia, 23504, USA

[20]North Carolina Central University, Durham, North Carolina, 27707, USA

[21]Old Dominion University, Norfolk, Virginia, 23529, USA

[22]Institut de Physique Nucléaire, F-91406 Orsay, France

[23]Princeton University, Princeton, New Jersey, 08544, USA

[24]University of Regina, Regina, Saskatchewan, Canada, S4S 0A2

[25]Rutgers, The State University of New Jersey, Piscataway, New Jersey, 08854, USA

[26] *CEA Saclay, F-91191 Gif-sur-Yvette, France*

[27] *State University of New York at Stony Brook, Stony Brook, New York, 11794, USA*

[28] *Syracuse University, Syracuse, New York, 13244, USA*

[29] *Temple University, Philadelphia, Pennsylvania, 19122, USA*

[30] *Thomas Jefferson National Accelerator Facility, Newport News, Virginia, 23606, USA*

[31] *Tohoku University, Sendai 980, Japan*

[32] *University of Virginia, Charlottesville, Virginia, 22901, USA*

[33] *College of William and Mary, Williamsburg, Virginia, 23187, USA*

[34] *Yamagata University, Yamagata 990, Japan*

[35] *Yerevan Physics Institute, Yerevan 375036, Armenia*

[36] *Universidad Complutense de Madrid, E-28040 Madrid, Spain*

(February 9, 2001)

Abstract

This section is currently under development.

self-calibrating; self-normalizing; first experiment in Hall A; bound states and continuum at $|\vec{q}| = 1$ GeV/c and $\omega = 0.445$ GeV.

PACS 25.30.Fj, 27.20.+n

I. INTRODUCTION

This section is currently under development.[1]

II. EXPERIMENT

This experiment [1,2] was the inaugural physics investigation performed in Hall A [3] (the High Resolution Hall) at the Thomas Jefferson National Accelerator Facility (JLab) [4]. An overview of the experiment apparatus present in the Hall at the time of this measurement is shown in Fig. 1.

A. Electron beam

Unpolarized 70-μA continuous electron beams with nominal energies of 0.845, 1.645, and 2.445 GeV and a typical $\pm 4\sigma$ energy spread of 0.01% were used for this experiment. Subsequent analysis of the data demonstrated that the actual beam energies were within 0.3% of the nominal values [5]. The typical laboratory horizontal (vertical) $\pm 4\sigma$ beam extent at the target was 0.5 mm (0.1 mm) . Beam current monitors [7] (calibrated using an Unser monitor [8]) were used to determine the total charge delivered to the target to an accuracy of 2% [9]. Beam position monitors (BPMs) [6] were used to ensure the location of the beam at the target was no more than 0.2 mm from the beamline axis, and that the instantaneous angle between the beam and the beamline axis was no larger than 0.15 mrad. The readout

[1] Kinematically, an electron scattered through angle θ_e transfers momentum $\vec{q}$ and energy ω with $Q^2 = \vec{q}^{\,2} - \omega^2$. The ejected proton has mass m_p, momentum $\vec{p}_p$, energy E_p, and kinetic energy T_p. The cross section is typically measured as a function of missing energy $E_{\rm miss} = \omega - T_p - T_{\rm recoil}$ and missing momentum $p_{\rm miss} = |\vec{q} - \vec{p}_p|$. The lab polar angle between the ejected proton and virtual photon is θ_{pq} and the azimuthal angle is ϕ. $\theta_{pq} > 0°$ corresponds to $\phi = 180°$ and $\theta_p > \theta_q$. $\theta_{pq} < 0°$ corresponds to $\phi = 0°$.

from the BCM and BPMs was continuously passed into the data stream [10]. Non-interacting electrons were dumped in a well-shielded, high-power beam dump [11] located roughly 25 m from the target.

B. Target

A waterfall target [12] positioned inside a scattering chamber located at the center of the Hall provided the H_2O used for this study of ^{16}O. The target canister was a rectangular box 20-cm long × 15-cm wide × 10-cm high containing air at atmospheric pressure. The beam entrance (exit) windows to this canister were 50-μm (75-μm) gold-plated beryllium foils. Inside the canister, three thin, parallel water films served as targets. This three-film configuration was superior to a single film 3×-thicker because it reduced the target-associated multiple scattering and energy loss. The films were defined by 2 mm × 2 mm stainless-steel posts. Each film was separated by 25 mm along the direction of the beam, and was rotated such that the normal to the film surface made an angle of 30° with respect to the beam direction. This geometry ensured particles originating from any given film would not intersect any other film on their way into the spectrometers. The thickness of the films could be changed by varying the speed of the water flow through the target circuit via a pump. The average film thicknesses were fixed at (130 ± 2.5%) mg/cm^2 along the direction of the beam throughout the experiment, which provided a good trade-off between resolution and target thickness. The thickness of the central water film was determined by comparing $^{16}\mathrm{O}(e,e')$ cross sections measured at $|\vec{q}| = 330$ MeV/c obtained from both the film and a (155 ± 1.5%) mg/cm^2 BeO target foil placed in a solid target ladder mounted beneath the target canister. The thicknesses of the side films were determined by comparing the concurrently measured $^1\mathrm{H}(e,e)$ cross sections obtained from the side films to that obtained from the central film. Instantaneous variations in the target film thicknesses were monitored throughout the entire experiment by continuously measuring the $^1\mathrm{H}(e,e)$ cross sections. The scattered electrons and knocked-out protons passed through the 25-μm thick stainless-steel canister side windows on their way into the spectrometers, depositing roughly 200 keV.

C. Spectrometers and detectors

The base apparatus used in the experiment was a pair of optically identical 4 GeV/c superconducting High Resolution Spectrometers (HRS) [13]. These spectrometers have a nominal 9% momentum bite and a FWHM momentum resolution $\Delta p/p$ of roughly 10^{-4}. The nominal laboratory horizontal (vertical) angular acceptance is ± 25 (± 50) mrad. Scattered electrons were detected in the Electron Spectrometer (HRS$_e$), and knocked-out protons were detected in the Hadron Spectrometer (HRS$_h$) (see Fig. 1). Before the experiment, the absolute momentum calibration of the spectrometers was determined to $\Delta p/p = 1.5 \times 10^{-3}$ [5]. Before and during the experiment, both the optical properties and acceptances of the spectrometers were studied [14]. Some optical parameters are presented in Table II. During the experiment, the spectrometers were surveyed to an accuracy of 0.3 mrad at every angular location [15]. The status of the magnets was continuously monitored and logged [10].

The detector packages were located in a well-shielded detector huts built on decks located above each spectrometer (approximately 25 m from the target and 15 m above the floor of the Hall). The bulk of the instrumentation electronics were also located in these huts, and operated remotely from the Counting House. The HRS$_e$ detector package consisted of a pair of trigger scintillator planes [16] used to create single-arm triggers, a Vertical Drift Chamber (VDC) package [17] used for particle tracking, and a Gas Čerenkov counter [18] used to distinguish between π^- and electron events. Identical elements, except for the Gas Čerenkov counter, were also present in the HRS$_h$ detector package. The status of the various detector subsystems was continuously monitored and logged [10]. The individual operating efficiencies of each of these three devices was >99%.

D. Electronics and data acquisition

For a given spectrometer, a coincidence between signals from the two trigger scintillator planes indicated a 'single-arm' event. Simultaneous HRS_e and HRS_h singles events were recorded as 'coincidence' events. The basic trigger logic [19] allowed the proportion of single-arm events written to the data stream to be varied by remotely setting prescalers. Enough HRS_e singles were taken for a 1% $H(e, e)$ cross section measurement at each kinematics. Each spectrometer had its own VME crate (for scalers) and FASTBUS crate (for ADCs and TDCs). The crates were managed by readout controllers (ROCs). In addition to overseeing the state of the run, a trigger supervisor (TS) generated the triggers which caused the ROCs to read out the crates on an event-by-event basis. The VME (scaler) crate was also read out every ten seconds. An event builder (EB) collected the resulting data shards into events. An analyzer/data distributer (ANA/DD) analyzed and/or sent these events to the disk of the data acquisition computer. The entire data acquistion system was managed using the inhouse software toolkit CODA [20].

Typical scaler events were about 0.5 kb in length. Typical single-arm events were also about 0.5 kb, while typical coincidence events were about 1.0 kb. The acquisition deadtime η was monitored by measuring the TS output-to-input ratio for each event type. The event rates were set by varying the prescale factors and the beam current such that the DAQ computer was dead at the most only 20% of the time. This resulted in a relatively low event rate (kHz), at which the electronics deadtime was <1%. Online analyzers [21] were used to monitor the quality of the data as it was taken. Eventually, the data were transferred to magnetic tape. The ultimate data analysis was performed at a LINUX CPU farm at MIT [22] using the analysis package ESPACE [23].

III. ANALYSIS

A. Timing corrections and particle identification

Identification of coincidence $(e, e'p)$ events was in general a straightforward process. Software corrections were applied to remove timing variations induced by the trigger scintillator circuit and thus sharpen all Time-of-Flight (ToF) peaks. These included corrections to proton flight times due to variations in the proton kinetic energies, and corrections for variations in the electron and proton path lengths through the spectrometers. Pion rejection was performed using a ToF cut for π^+s in the HRS$_h$ and the Gas Čerenkov for π^-s in the HRS$_e$. A sharp, clear coincidence ToF peak with a FWHM of 1 ns and a typical signal-to-noise ratio of 5:1 resulted (see Fig. FF). High energy correlated protons which punched through the HRS$_h$ collimator (<10% of the prompt yield) were identified by requiring both spectrometers to independently reconstruct the coincidence event vertex in the vicinity of the same water film. The resulting prompt peak yields for each water film were corrected for uncorrelated (random) events present in the peak timing region on a bin-by-bin basis [24]. These per-film yields were then normalized individually.

B. Normalization

The relative focal plane efficiencies for each of the two spectrometers were measured independently for each of the three water films at every spectrometer excitation used in the experiment. By measuring the same single-arm cross section at different positions across the spectrometer focal planes, variations in the relative efficiency were identified. The position variation across the focal plane was investigated by systematically shifting the central excitation of the spectrometer in a series of discrete steps about the mean momentum setting such that the full momentum acceptance was mapped. A smooth, slowly varying dip-region cross section was used instead of a single discrete peak for continuous coverage of the focal plane. The relative efficiency profiles were unfolded from these data using the program REL-

EFF [25]. For each water film, solid angle cuts were then applied to select the flat regions of the angular acceptance. These cuts reduced the spectrometer apertures by roughly 20% to about 4.8 msr. Finally, relative momentum cuts were applied to select the flat regions of momentum acceptance. These cuts reduced the spectrometer momentum acceptance by roughly 22% to -3.7% $< \delta <$ 3.3%. The resulting acceptance profile of each spectrometer was uniform to within 1%.

The absolute efficiency at which the two spectrometers operated in coincidence mode was given by

$$\epsilon = \epsilon_e \; \epsilon_p \; \epsilon_{coin}, \tag{1}$$

where ϵ_e was the single-arm HRS$_e$ efficiency, ϵ_p was the single-arm HRS$_h$ efficiency, and ϵ_{coin} was the coincidence trigger efficiency. The quantity ($\epsilon_p \; \epsilon_{coin}$) was measured in parallel kinematics at $E_{\rm beam}$ = 0.845 GeV using the H(e, ep) reaction. A 0.7 msr collimator was placed in front of the HRS$_e$. In these kinematics, the cone of recoil protons fit entirely into the central flat acceptance region of the HRS$_h$. The number of H(e, e) events where the proton was detected was compared to the number of H(e, e) events where it was not to yield a product of efficiencies $\epsilon_p \; \epsilon_{coin}$ of 98.9%. The 1.1% effect was due to proton absorption in the waterfall target exit windows, spectrometer windows, and the first layer of trigger scintillators. Since the central field of the HRS$_h$ was held constant throughout the entire experiment, this measurement was applicable to each of the hadron kinematics employed. A similar method was used to determine the quantity ($\epsilon_e \; \epsilon_{coin}$) at each of the three HRS$_e$ field settings. Instead of a collimator, software cuts applied to the recoil protons were used to ensure the cone of scattered electrons fit entirely into the central flat acceptance region of the HRS$_e$. This product of efficiencies was >99%. Thus, the coincidence efficiency ϵ_{coin} was firmly established at nearly 100%. A nominal sytematic uncertainty of ±1% was assigned to ϵ.

The quantity ($\ell \; \epsilon_e$), where ℓ is the luminosity (the product of the effective target thickness and the number of incident electrons) was determined to ±4% by comparing the measured

H(e, e) cross section for each film at each of the electron kinematics to a parametrization established at a similar Q^2 [26]. The results reported in this paper have all been normalized in this fashion. As a consistency check, direct calculation of $(\ell\ \epsilon_e)$ using information from the BCMs, the calibrated thicknesses of the water films, and the single-arm HRS$_e$ efficiency agrees within error.

At every kinematics, a Monte Carlo of the phase space volume subtended by each experimental bin was performed. For each water foil, N_0 software $(e, e'p)$ events were generated, uniformly distributed over the scattered electron and knocked-out proton momenta $(p_e,\ p_p)$ and in-plane and out-of-plane angles $(\phi_e,\ \theta_e,\ \phi_p,\ \theta_p)$. For each of these events, all of the kinematic quantities were calculated. The flat-acceptance cuts determined in the analysis of the relative focal plane efficiency data were then applied, as were all other cuts that had been performed on the actual data. The detection volume $\Delta V_b(E_{\rm miss},\ p_{\rm miss},\ \omega,\ Q^2)$ subtended by a bin $b(\Delta E_{\rm miss},\ \Delta p_{\rm miss},\ \Delta\omega,\ \Delta Q^2)$ containing N_b pseudoevents was thus

$$\Delta V_b(E_{\rm miss}, p_{\rm miss}, \omega, Q^2) = \frac{N_b}{N_0} \times\ [(\Delta p_e \cdot \Delta\Omega_e)\cdot(\Delta p_p \cdot \Delta\Omega_p)], \tag{2}$$

where the quantity $(\Delta p_e \cdot \Delta\Omega_e)\cdot(\Delta p_p \cdot \Delta\Omega_p)$ was the total volume sampled over in the Monte Carlo (purposely set larger than the experimental acceptance in all dimensions). In order to change the differential dependencies of the measured cross sections to match those employed in theoretical calculations, the pristine detection volume $\Delta V_b(E_{\rm miss},\ p_{\rm miss},\ \omega,\ Q^2)$ could be converted to a weighted detection volume $\Delta V_b'(E_{\rm miss},\ p_{\rm miss},\ \omega,\ Q^2)$ by weighting each of the trials with the appropriate Jacobian(s). The pseudodata were binned exactly as the real data, and uniformly on both sides of $\vec{q}$. At each kinematics, the bin with the largest volume $\Delta V_{\rm max}$ was located. Only bins subtending volumes larger than 50% of $\Delta V_{\rm max}$ were analyzed further.

Corrections based on the TS output-to-input ratio were applied to account for the acquisition deadtime to coincidence events. On average, these corrections were roughly 20%. An acquisition Monte Carlo [27] was used to cross-check these corrections and establish the absolute uncertainty in them at 2%.

Corrections to the per-film cross sections for electron radiation before and after scattering were calculated using both a modified version of the code RADCOR [28] and independently, the prescriptions contained within the simulation package MCEEP [29] on a bin-by-bin basis. The two approaches agreed to within the statistical uncertainty of the data and amounted to <55% (<15%) of the measured cross section for the bound states (continuum). Corrections for proton radiation at these energies are much less than 1% and were not performed.

C. Systematic uncertainties

This section is currently under development. Please see the various tables summarizing the work done so far which come at the end of this draft.

IV. RESULTS AND DISCUSSION

A. Cross sections

This section is currently under development.

The radiatively corrected average cross section in the bin $b(\Delta E_{\rm miss},\ \Delta p_{\rm miss},\ \Delta\omega,\ \Delta Q^2)$ was calculated according to

$$\left\langle \frac{d^6\sigma}{d\omega\ d\Omega_e\ dE_{\rm miss}\ d\Omega_p} \right\rangle_b = \frac{1}{(\ell\ \epsilon_e)(\epsilon_p\ \epsilon_{coin})} \cdot \left(\frac{Y_b}{\Delta V_b'} \right) \cdot \eta \cdot R, \tag{3}$$

where Y_b was the total number of real events which were detected in $b(\Delta E_{\rm miss},\ \Delta p_{\rm miss},\ \Delta\omega,\ \Delta Q^2)$, η was a correction applied to account for the deadtime of the electronics and the acquisiton system to coincidence events, and R was a correction applied to account for events which radiated out of $\Delta V_b'$. The average cross section was calculated as a function of $E_{\rm miss}$ for a given kinematic setting. Bound state cross sections were extracted by integrating over the appropriate range in $E_{\rm miss}$. The bound state (continuum) cross sections are presented in Table XX (YY).

Discussion of cross section results here.

Response function separations were performed where the phase space overlap between kinematics permitted [30,31]. For these separations, bins were selected only if their their phase space volumes $\Delta V_b'$ were all simultaneously 50% of $\Delta V_{\max}$.

Discussion of structure function results here.

The interested reader is directed to [32,33] for complete details of the data analysis.

V. SUMMARY AND CONCLUSIONS

This section is currently under development.

ACKNOWLEDGEMENTS

We acknowledge the outstanding support of the staff of the Accelerator and Physics Divisions at Jefferson Laboratory that made this experiment successful. We thank T. W. Donnelly, J. Ryckebusch, and J. W. Van Orden for providing theoretical calculations and for valuable discussions. This work was supported in part by the U. S. Department of Energy contract DE-AC05-84ER40150 under which the Southeastern Universities Research Association (SURA) operates the Thomas Jefferson National Accelerator Facility, other Department of Energy contracts, the National Science Foundation, the Italian Istituto Nazionale di Fisica Nucleare (INFN), the French Atomic Energy Commission and National Center of Scientific Research, and the Natural Sciences and Engineering Research Council of Canada.

REFERENCES

[1] A. Saha, W. Bertozzi, R.W. Lourie, and L.B. Weinstein, *A Study of the Quasielastic $(e, e'p)$ Reaction in ^{16}O at High Recoil Momentum*, Jefferson Laboratory Proposal 89-003, 1989; see also `www.jlab.org/exp_prog/experiments/summaries/`

[2] K.G Fissum *et al.*, *A Study of the Quasielastic $(e, e'p)$ Reaction in ^{16}O at High Recoil Momentum*, MIT-LNS Internal Report No. 2, 1997 (unpublished); see also `www.jlab.org/~fissum/e89003.html`

[3] `hallaweb.jlab.org/`

[4] `www.jlab.org`

[5] J. Gao *et al.*, *Beam Energy Measurement at Jefferson Lab Using the Hall A Spectrometers*, MIT-LNS Internal Report No. 4, 1998 (unpublished); see also `www.jlab.org/~fissum/e89003/learned/e89003-beamdel.ps.gz`

[6] need BPM reference

[7] need BCM reference

[8] K.B. Unser, *Design and Preliminary Test of a Beam Intensity Monitor for LEP*, Proc. IEEE Particle Accelerator Conference, Chicago, IL, **71** (1989).

[9] P.E. Ulmer, *Beam Current Measurements - Experiment E89-003 at Jefferson Laboratory*, 1998 (unpublished); see also `www.jlab.org/~fissum/e89003/learned/e89003-charge.ps.gz`

[10] need EPICS reference

[11] need beamdump reference

[12] F. Garibaldi *et al.*, Nucl. Instrum. Meth. **A314**, 1 (1992).

[13] `hallaweb.jlab.org/equipment/high_resol.html`

[14] N. Liyanage, *Optics Commissioning of the Hall A High Resolution Spectrometers*, MIT-LNS Internal Report No. 5, 1998 (unpublished); see also www.jlab.org/~fissum/e89003/learned/e89003-optics.ps.gz

[15] M. Liang, *Survey Summary Report*, Jefferson Lab Technical Notes No. JLAB-TN-99029, 1998 (unpublished);

[16] hallaweb.jlab.org/equipment/detectors/detectors.html; hallaweb.jlab.org/equipment/detectors/trig.html;

[17] K. G. Fissum *et al.*, submitted to Nucl. Instrum. Meth. (2000); see also www.jlab.org/~fissum/vdcs.html

[18] M. Iodice *et al.*, Nucl. Instrum. Meth. **A411**, 223 (1998); see also hallaweb.jlab.org/equipment/detectors/gas.html

[19] hallaweb.jlab.org/equipment/acquisition.html

[20] coda.jlab.org/

[21] hallaweb.jlab.org/equipment/daq/dplot.html

[22] wizard.mit.edu/ ~wwc/abacus.html

[23] hallaweb.jlab.org/espace/index.html

[24] R. O. Owens, Nucl. Instrum. Meth. **A288**, 574 (1990)

[25] L. B. Weinstein, Ph.D. thesis, Massachusetts Institute of Technology, 1988 (unpublished)

[26] G.G. Simon *et al.*, Nucl. Phys. **A333**, 381 (1980); L.E. Price *et al.*, Phys. Rev **D4**, 45 (1971).

[27] www.jlab.org/ ~mliang/deadtime_cor/

[28] E. Quint, Ph.D. thesis, University of Amsterdam, 1988 (unpublished); R. Florizone,

Ph.D. thesis, Massachusetts Institute of Technology, 1999 (unpublished).

[29] `www.physics.odu.edu/ ~ulmer/mceep/mceep.html`; see also E. Borie and D. Drechsel, Nucl. Phys. **A167**, 369 (1971) and J. Templon *et al.*, Phys. Rev. **C61**, 014607 (2000).

[30] J. Gao *et al.*, Phys. Rev. Lett. **84**, 3265 (2000).

[31] N. Liyanage *et al.*, submitted to Phys. Rev. Lett. (2000).

[32] J. Gao, Ph.D. thesis, Massachusetts Institute of Technology, 1999 (unpublished).

[33] N. Liyanage, Ph.D. thesis, Massachusetts Institute of Technology, 1999 (unpublished).

FIGURES

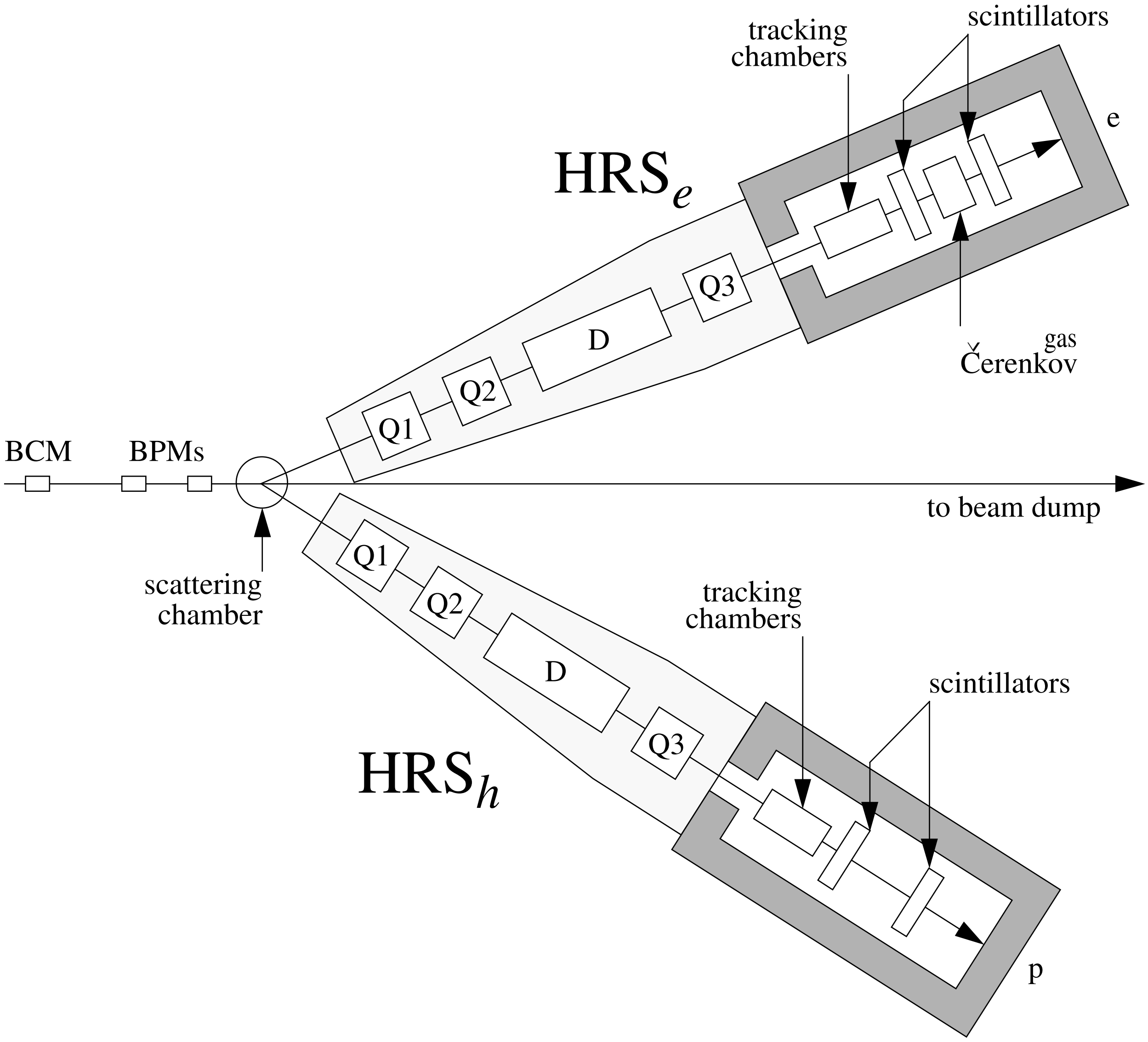

FIG. 1. Hall A at Jefferson Lab at the time of this experiment. The electron beam passed through a beam current monitor (BCM) and beam position monitors (BPMs) before striking a waterfall target located in the scattering chamber. Scattered electrons were detected in the HRS_e, while knocked-out protons were detected in the HRS_h. Non-interacting electrons were dumped. The spectrometers were free to rotate about the central pivot.

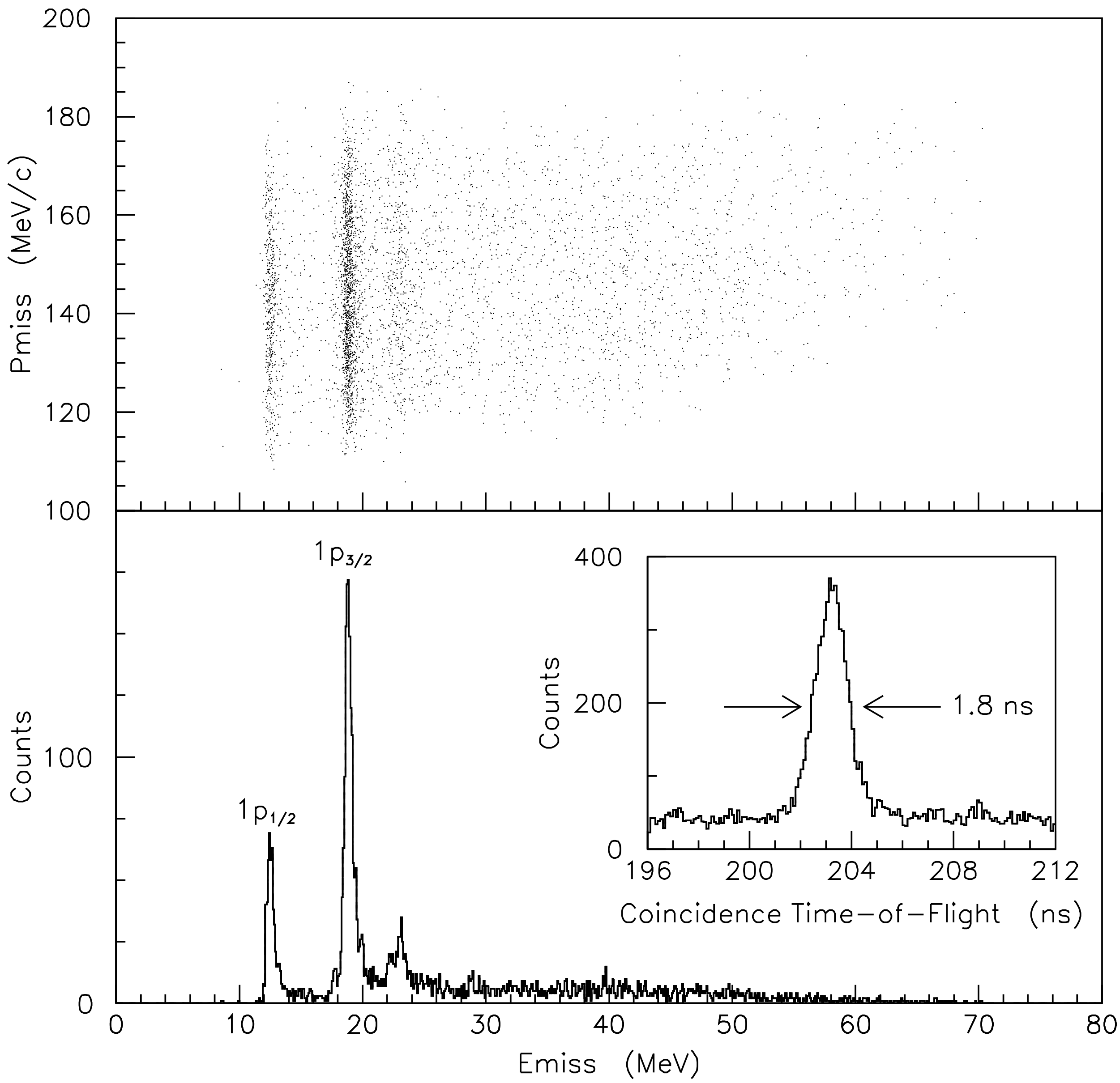

FIG. 2. Yield spectra obtained at $E_{\mathrm{beam}} = 0.845$ GeV and $\theta_{pq} = +8^{\circ}$. Pion rejection has been performed, and all timing corrections have been applied. The top panel shows a scatterplot of p_{miss} versus E_{miss}. The dark vertical bands project into the peaks located at 12.1 (18.3) MeV in the bottom panel. These peaks correspond to protons knocked-out of the $1p_{1/2}$- ($1p_{3/2}$-) state of ^{16}O. The bump located at roughly 23 MeV is a negative-parity doublet which was not investigated. The insert shows the corresponding optimized coincidence time-of-flight peak which has a FWHM of 1.8 ns. The signal-to-noise ratio was about 8:1 in these kinematics.

TABLES

TABLE I. Experiment kinematics. These quasielastic parameters were established within a constant center-of-mass energy framework. At each beam energy, $|\vec{q}|$ = 1 GeV/c. The angles θ_{pq} = 0, ±2.5, ±8, ±16, and ±20° correspond to central missing momenta of 53, 60, 148, 280, and 345 MeV/c, respectively.

E_{beam} (GeV)	θ_e (°)	θ_{pq} (°)
0.845	100.76	0, 8, 16
1.645	37.17	0, ±8
2.445	23.36	0, ±2.5, ±8, ±16, ±20

TABLE II. Results of the optics commissioning measurements.

parameter	resolution (FWHM)	reconstruction accuracy
out-of-plane angle	6.00 mrad	±0.60 mrad
in-plane angle	2.30 mrad	±0.23 mrad
y_{target}	2.00 mm	±0.20 mm
$\Delta p/p$	2.5×10^{-4}	$\pm 0.25 \times 10^{-4}$

TABLE III. Summary of the energy-independent systematic uncertainties.

Quantity	$\delta^{\mathrm{systematic}}$
$\rho \cdot t'$	2.5%
N_e	2.0%
ℓ	3.2%
ϵ_e	1.0%
$(\ell \cdot \epsilon_e)$	4.0%
$(\epsilon_p \cdot \epsilon_{coin})$	1.1%
$\Delta\Omega_e$	2.0%
$(\Delta\Omega_p)$	2.0%
dt	1.0%
radiative corrections	

TABLE IV. Summary of the energy- and momentum-dependent systematic uncertainties due to an uncertainty in the absolute beam energy of 1.6×10^{-3}. 10k (1 M) events were simulated and the cross sections were averaged over the entire acceptance. Numbers labeled with a † should not be taken too seriously.

			$\delta(d^5\sigma/d\omega d\Omega_e d\Omega_p)$	$\delta(d^6\sigma/d\omega dE_p d\Omega_e d\Omega_p)$
$E_{\rm beam}$	θ_{pq}	$1p_{1/2}$-state	$1p_{3/2}$-state	continuum
(GeV)	(°)	(%)	(%)	(%)
0.843	0	1.2 (1.3)	1.4 (1.3)	0.1 (<0.1)
	8	0.9 (0.9)	1.0 (1.1)	1.6 (1.6)
	16	1.9 (1.5)	3.2 (3.2)	$3.7^{\dagger}$ $(3.7)^{\dagger}$
1.642	-8	2.3 (2.5)	2.2 (2.2)	2.6 (2.9)
	0	0.4 (0.7)	0.9 (1.0)	1.4 (1.3)
	8	0.8 (0.7)	0.5 (0.6)	0.4 (0.3)
2.442	-20	5.9 (5.3)	4.4 (4.9)	$5.2^{\dagger}$ $(6.0)^{\dagger}$
	-16	3.8 (3.9)	3.2 (3.6)	$4.0^{\dagger}$ $(4.3)^{\dagger}$
	-8	2.6 (2.4)	2.1 (2.1)	2.8 (2.8)
	-2.5	1.0 (1.0)	0.9 (0.8)	1.7 (1.3)
	0	0.3 (0.4)	0.3 (0.2)	1.2 (0.5)
	2.5	0.3 (0.4)	0.4 (0.3)	1.0 (0.2)
	8	0.2 (0.4)	0.6 (0.5)	0.4 (0.3)
	16	0.6 (0.1)	0.3 (<0.1)	$0.4^{\dagger}$ $(0.5)^{\dagger}$
	20	0.9 (0.3)	0.7 (0.3)	$1.4^{\dagger}$ $(0.8)^{\dagger}$

TABLE V. Summary of the energy- and momentum-dependent systematic uncertainties due to an uncertainty in the absolute electron angle of 0.3 mrad. 10k (1 M) events were simulated and the cross sections were averaged over the entire acceptance. Numbers labeled with a † should not be taken too seriously.

			$\delta(d^5\sigma/d\omega d\Omega_e d\Omega_p)$	$\delta(d^6\sigma/d\omega dE_p d\Omega_e d\Omega_p)$
E_{beam}	θ_{pq}	$1p_{1/2}$-state	$1p_{3/2}$-state	continuum
(GeV)	(°)	(%)	(%)	(%)
0.843	0	0.3 (<0.1)	0.9 (0.1)	0.1 (0.1)
	8	0.2 (0.2)	0.2 (0.2)	0.3 (0.3)
	16	0.4 (0.4)	0.4 (0.4)	$0.5^{\dagger}$ $(0.3)^{\dagger}$
1.642	-8	0.6 (0.6)	0.5 (0.5)	0.6 (0.6)
	0	0.1 (<0.1)	0.1 (0.1)	0.5 (0.5)
	8	0.4 (0.4)	0.4 (0.4)	0.5 (0.5)
2.442	-20	2.0 (2.0)	1.9 (1.8)	$2.2^{\dagger}$ $(2.2)^{\dagger}$
	-16	1.5 (1.5)	1.4 (1.4)	$1.6^{\dagger}$ $(1.5)^{\dagger}$
	-8	1.0 (1.0)	0.9 (0.9)	1.1 (1.1)
	-2.5	0.6 (0.6)	0.5 (0.5)	0.9 (0.8)
	0	0.4 (0.4)	0.3 (0.3)	0.8 (0.7)
	2.5	0.5 (0.5)	0.4 (0.4)	0.7 (0.7)
	8	0.6 (0.6)	0.6 (0.6)	0.6 (0.6)
	16	0.6 (0.6)	0.6 (0.6)	$0.6^{\dagger}$ $(0.6)^{\dagger}$
	20	0.6 (0.6)	0.6 (0.6)	$0.7^{\dagger}$ $(0.7)^{\dagger}$

TABLE VI. Summary of the energy- and momentum-dependent systematic uncertainties due to an uncertainty in the absolute hadron angle of 0.3 mrad. 10k (1 M) events were simulated and the cross sections were averaged over the entire acceptance. Numbers labeled with a † should not be taken too seriously.

			$\delta(d^5\sigma/d\omega d\Omega_e d\Omega_p)$	$\delta(d^6\sigma/d\omega dE_p d\Omega_e d\Omega_p)$
E_{beam}	θ_{pq}	$1p_{1/2}$-state	$1p_{3/2}$-state	continuum
(GeV)	(°)	(%)	(%)	(%)
0.843	0	0.2 (0.1)	0.1 (<0.1)	0.1 (<0.1)
	8	0.5 (0.5)	0.4 (0.4)	0.7 (0.7)
	16	1.2 (1.2)	1.0 (1.0)	1.3† (1.3)†
1.642	-8	0.7 (0.7)	0.4 (0.5)	0.7 (0.7)
	0	0.2 (0.2)	0.1 (0.1)	0.1 (<0.1)
	8	0.4 (0.4)	0.3 (0.3)	0.7 (0.7)
2.442	-20	1.8 (1.7)	1.6 (1.5)	1.9† (1.9)†
	-16	1.3 (1.3)	1.1 (1.1)	1.3† (1.3)†
	-8	0.7 (0.7)	0.5 (0.5)	0.8 (0.7)
	-2.5	0.3 (0.3)	0.2 (0.2)	0.3 (0.3)
	0	0.1 (0.1)	0.1 (<0.1)	0.1 (<0.1)
	2.5	0.2 (0.2)	0.2 (0.2)	0.3 (0.3)
	8	0.5 (0.4)	0.3 (0.3)	0.7 (0.7)
	16	1.1 (1.0)	1.0 (0.9)	1.4† (0.4)†
	20	1.5 (1.5)	1.5 (1.4)	2.2† (2.1)†

TABLE VII. Summary of the energy- and momentum-dependent systematic uncertainties due to an uncertainty in the absolute electron momentum of 1.5×10^{-3}. 10k (1 M) events were simulated and the cross sections were averaged over the entire acceptance. Numbers labeled with a † should not be taken too seriously.

		$\delta(d^5\sigma/d\omega d\Omega_e d\Omega_p)$		$\delta(d^6\sigma/d\omega dE_p d\Omega_e d\Omega_p)$
E_{beam}	θ_{pq}	$1p_{1/2}$-state	$1p_{3/2}$-state	continuum
(GeV)	(°)	(%)	(%)	(%)
0.843	0	1.4 (1.3)	1.6 (1.5)	0.9 (0.9)
	8	0.2 (0.2)	0.2 (0.2)	0.2 (0.2)
	16	0.8 (0.8)	1.1 (1.2)	$1.2^{\dagger}$ $(1.4)^{\dagger}$
1.642	-8	0.3 (<0.1)	0.1 (<0.1)	0.1 (<0.1)
	0	0.5 (0.7)	0.2 (<0.1)	0.1 (<0.1)
	8	0.3 (0.2)	0.1 (<0.1)	0.2 (<0.1)
2.442	-20	0.6 (<0.1)	0.1 (<0.1)	$0.5^{\dagger}$ $(0.2)^{\dagger}$
	-16	0.3 (<0.1)	0.4 (<0.1)	$0.6^{\dagger}$ $(0.2)^{\dagger}$
	-8	0.2 (<0.1)	0.2 (<0.1)	0.1 (0.1)
	-2.5	0.2 (<0.1)	0.2 (<0.1)	0.2 (<0.1)
	0	0.2 (<0.1)	0.1 (<0.1)	0.2 (<0.1)
	2.5	0.2 (<0.1)	0.1 (<0.1)	0.3 (<0.1)
	8	0.2 (<0.1)	0.1 (<0.1)	0.3 (0.1)
	16	0.4 (<0.1)	0.2 (<0.1)	$0.7^{\dagger}$ $(0.1)^{\dagger}$
	20	0.9 (0.2)	0.5 (<0.1)	$1.3^{\dagger}$ $(0.3)^{\dagger}$

TABLE VIII. Summary of the energy- and momentum-dependent systematic uncertainties due to an uncertainty in the absolute hadron momentum of 1.5×10^{-3}. 10k (1 M) events were simulated and the cross sections were averaged over the entire acceptance. Numbers labeled with a † should not be taken too seriously.

			$\delta(d^5\sigma/d\omega d\Omega_e d\Omega_p)$	$\delta(d^6\sigma/d\omega dE_p d\Omega_e d\Omega_p)$
$E_{\rm beam}$	θ_{pq}	$1p_{1/2}$-state	$1p_{3/2}$-state	continuum
(GeV)	(°)	(%)	(%)	(%)
0.843	0	0.3 (0.2)	0.3 (0.2)	0.1 (<0.1)
	8	0.5 (0.5)	0.1 (0.1)	0.1 (<0.1)
	16	1.4 (1.4)	0.1 (0.1)	$0.1^{\dagger}$ $(0.1)^{\dagger}$
1.642	-8	2.1 (2.2)	1.8 (2.8)	2.2 (2.5)
	0	1.2 (1.2)	1.4 (2.5)	0.7 (0.7)
	8	0.7 (0.9)	0.6 (0.6)	2.2 (1.7)
2.442	-20	4.0 (3.8)	3.7 (3.4)	$4.6^{\dagger}$ $(4.4)^{\dagger}$
	-16	3.7 (3.1)	2.4 (2.7)	$3.2^{\dagger}$ $(3.4)^{\dagger}$
	-8	2.0 (2.0)	1.6 (1.6)	2.0 (2.3)
	-2.5	0.8 (0.8)	0.6 (0.8)	0.9 (1.1)
	0	0.2 (0.2)	0.2 (0.4)	0.4 (0.5)
	2.5	0.5 (0.5)	0.4 (0.5)	0.8 (0.9)
	8	1.0 (1.1)	0.7 (0.7)	1.7 (1.8)
	16	3.9 (3.2)	3.1 (2.9)	$4.4^{\dagger}$ $(4.3)^{\dagger}$
	20	5.0 (4.9)	4.6 (4.6)	$7.6^{\dagger}$ $(7.2)^{\dagger}$

TABLE IX. Quadratic sum of the energy- and momentum-dependent systematic uncertainties. 10k (1 M) events were simulated and the cross sections were averaged over the entire acceptance. Numbers labeled with a † should not be taken too seriously.

		$\delta(d^5\sigma/d\omega d\Omega_e d\Omega_p)$		$\delta(d^6\sigma/d\omega dE_p d\Omega_e d\Omega_p)$
$E_{\rm beam}$	θ_{pq}	$1p_{1/2}$-state	$1p_{3/2}$-state	continuum
(GeV)	(°)	(%)	(%)	(%)
0.843	0	1.9 (1.9)	2.3 (2.0)	0.9 (0.9)
	8	1.2 (1.2)	1.1 (1.2)	1.8 (1.8)
	16	2.8 (2.5)	3.6 (3.6)	$4.1^{\dagger}$ $(4.2)^{\dagger}$
1.642	-8	3.3 (3.5)	2.9 (3.6)	3.5 (3.9)
	0	1.4 (1.6)	1.7 (2.7)	1.7 (1.6)
	8	1.2 (1.3)	0.9 (1.0)	2.4 (1.9)
2.442	-20	7.6 (7.0)	6.3 (6.4)	$7.5^{\dagger}$ $(8.0)^{\dagger}$
	-16	5.7 (5.4)	4.4 (4.8)	$5.6^{\dagger}$ $(5.8)^{\dagger}$
	-8	3.5 (3.4)	2.8 (2.8)	3.7 (3.9)
	-2.5	1.5 (1.4)	1.2 (1.3)	2.2 (1.9)
	0	0.6 (0.6)	0.5 (0.5)	1.5 (1.0)
	2.5	0.8 (0.8)	0.7 (0.7)	1.5 (1.2)
	8	1.3 (1.4)	1.1 (1.1)	2.0 (2.0)
	16	4.2 (3.4)	3.3 (3.1)	$4.7^{\dagger}$ $(4.4)^{\dagger}$
	20	5.4 (5.2)	5.0 (4.9)	$8.2^{\dagger}$ $(7.6)^{\dagger}$

TABLE X. Summary of the energy- and momentum-dependent systematic uncertainties in the H(e,e) cross section due to an uncertainty in the absolute beam energy of 1.6×10^{-3}. 1 M events were simulated and the cross sections were averaged over the HRS$_e$ acceptance.

E_{beam} (GeV)	θ_e ($^\circ$)	$\delta(d\sigma/d\Omega_e)$ (%)
0.843	100.76	0.7
1.642	37.17	0.7
2.442	23.36	0.6

TABLE XI. Summary of the energy- and momentum-dependent systematic uncertainties in the H(e,e) cross section due to an uncertainty in the absolute electron angle of 0.3 mrad. 1 M events were simulated and the cross sections were averaged over the HRS$_e$ acceptance.

E_{beam} (GeV)	θ_e ($^\circ$)	$\delta(d\sigma/d\Omega_e)$ (%)
0.843	100.76	0.1
1.642	37.17	0.4
2.442	23.36	0.9

TABLE XII. Summary of the energy- and momentum-dependent systematic uncertainties in the H(e,e) cross section due to an uncertainty in the absolute electron momentum of 1.5×10^{-3}. 1 M events were simulated and the cross sections were averaged over the HRS$_e$ acceptance.

E_{beam} (GeV)	θ_e ($^\circ$)	$\delta(d\sigma/d\Omega_e)$ (%)
0.843	100.76	0.1
1.642	37.17	0.1
2.442	23.36	<0.1

TABLE XIII. Summary of the energy- and momentum-dependent systematic uncertainties in the H(e,e) cross section due to an uncertainty in the absolute beam energy of 1.6×10^{-3}. 1 M events were simulated and the HRS$_h$ acceptance was enforced. The cross sections were averaged over the HRS$_e$ acceptance.

E_{beam} (GeV)	θ_e ($^\circ$)	θ_h ($^\circ$)	$\delta(d\sigma/d\Omega_e)$ (%)
0.843	100.76	23.12	<0.1
1.642	37.17	46.45	0.2
2.442	23.36	52.47	0.1

TABLE XIV. Summary of the energy- and momentum-dependent systematic uncertainties in the H(e,e) cross section due to an uncertainty in the absolute electron angle of 0.3 mrad. 1 M events were simulated and the HRS$_h$ acceptance was enforced. The cross sections were averaged over the HRS$_e$ acceptance.

E_{beam} (GeV)	θ_e ($^\circ$)	θ_h ($^\circ$)	$\delta(d\sigma/d\Omega_e)$ (%)
0.843	100.76	23.12	<0.1
1.642	37.17	46.45	0.1
2.442	23.36	52.47	0.2

TABLE XV. Summary of the energy- and momentum-dependent systematic uncertainties in the H(e,e) cross section due to an uncertainty in the absolute electron momentum of 1.5×10^{-3}. 1 M events were simulated and the HRS$_h$ acceptance was enforced. The cross sections were averaged over the HRS$_e$ acceptance..

E_{beam} (GeV)	θ_e (°)	θ_h (°)	$\delta(d\sigma/d\Omega_e)$ (%)
0.843	100.76	23.12	<0.1
1.642	37.17	46.45	<0.1
2.442	23.36	52.47	<0.1

TABLE XVI. Summary of the energy- and momentum-dependent systematic uncertainties in the H(e,e) cross section due to an uncertainty in the absolute hadron angle of 0.3 mrad. 1 M events were simulated and the HRS$_h$ acceptance was enforced. The cross sections were averaged over the HRS$_e$ acceptance.

E_{beam} (GeV)	θ_e (°)	θ_h (°)	$\delta(d\sigma/d\Omega_e)$ (%)
0.843	100.76	23.12	<0.1
1.642	37.17	46.45	<0.1
2.442	23.36	52.47	0.1

TABLE XVII. Summary of the energy- and momentum-dependent systematic uncertainties in the H(e,e) cross section due to an uncertainty in the absolute hadron momentum of 1.5×10^{-3}. 1 M events were simulated and the HRS$_h$ acceptance was enforced. The cross sections were averaged over the HRS$_e$ acceptance.

$E_{\rm beam}$ (GeV)	θ_e (°)	θ_h (°)	$\delta(d\sigma/d\Omega_e)$ (%)
0.843	100.76	23.12	0.7
1.642	37.17	46.45	0.8
2.442	23.36	52.47	0.6

TABLE XVIII. Quadratic sum of the energy- and momentum-dependent systematic uncertainties. 1 M events were simulated and the HRS$_h$ acceptance was enforced. The cross sections were averaged over the HRS$_e$ acceptance.

$E_{\rm beam}$ (GeV)	θ_e (°)	θ_h (°)	$\delta(d\sigma/d\Omega_e)$ (%)
0.843	100.76	23.12	0.7
1.642	37.17	46.45	0.8
2.442	23.36	52.47	0.6